

Evaluation of mooring chain durability and system design method for Fukushima floating offshore wind farm

Hiroshi OOKUBO

Senior Manager, Design and Engineering Section,
Engineering Department,
Marine Engineering and Construction Division,
Nippon Steel Engineering Co. Ltd. (NSE).

Masahiko KANNO

Senior Manager, Design and Engineering Section,
Engineering Department,
Marine Engineering and Construction Division,
NSE.

Asuka KOIZUMI

Staff, Design and Engineering Section,
Engineering Department,
Marine Engineering and Construction Division,
NSE.

Nobuyuki HAYASHI

Senior Manager,
Plant Facility Smart Cleaning Department,
Business Solution Center,
NSE.

Kentaroh YAGI

Manager, Project Management Team,
Engineering Department,
Nippon Steel Steel Structure Co., Ltd.

Atsuo OOTAKE

Senior Manager,
Offshore Wind Design Section,
Engineering Department,
Marine Engineering and Construction Division,
NSE.

Mikio SUZUKI

Engineering Department Chief,
Nippon Steel Steel Structure Co., Ltd.

Abstract

The Fukushima Floating Offshore Wind Farm Demonstration Project¹⁾ was conducted by the Fukushima Offshore Wind Consortium to demonstrate the practical application of floating offshore wind turbines (FOWTs). Installation was at a site off the coast of Fukushima, with a water depth of approximately 120 m and severe metocean conditions having strong currents and tides, as well as high waves. A chain spread mooring system (SMS) was adopted for FOWT stationkeeping. In addition to the harsh marine environment, this system is subject to constant wind loads from turbine power production, complicating regular inspection and maintenance. However, reliable stationkeeping is of utmost importance, as a 20-year service life is expected for FOWTs. As part of the Nippon Steel Group, Nippon Steel Engineering Co., Ltd. (NSE) was given the opportunity to participate in the project, Demonstration Study on Steel Materials for FOWTs and Study on Life Evaluation of Mooring Chains. We created an abrasion and fatigue strength calculation method using material abrasion test results and finite element method (FEM) analysis, and we used measured data of floating substructure motions to calculate the abrasion amount and fatigue damage to mooring chains. We hereby report on our investigation and present new findings on the applicability of this mooring design method.

1 Introduction

Floating offshore wind turbines (FOWTs) are expected to be used in the waters on the continental shelf around Japan. FOWTs are considered economically viable in waters at depths ranging from 50 to 200 m. Therefore, the Fukushima Offshore Wind Farm Demonstration Project¹⁾ (hereinafter, “Fukushima FORWARD”) was established by the Fukushima Offshore Wind Consortium. This project is located at an offshore point off the coast of Fukushima, where the water depth is approximately 120 m, the Kuroshio and Oyashio currents meet, and the Pacific swells intersect, posing major hurdles for structure design, construction, and maintenance.

Compared to land-based wind turbines, FOWTs are more economically efficient as turbine facilities may be easily expanded through the use of marine transport²⁾. Fukushima FORWARD involves the installation of 2 to 7 MW wind turbines on floating substructures with displacement of 5,000 to 30,000 tons. In contrast, oil and gas production facilities involve the construction of floating production, storage, and offloading (FPSO) systems weighing hundreds of thousands of tons in marine areas where the water depth ranges from 200 to 3000 m. In comparison, the scale of and installation water depth of FOWTs are both smaller and only require the wind turbines. FOWTs are thus generally considered easy-to-build. On one hand, FPSOs are large-scale platforms equipped with facilities for oil and gas production, storage tanks, and offloading, and therefore, their construction presumes the use of large work barges. On the other hand, FOWTs preferably involve the installation of multiple platforms of similar size mutually spread apart at regular intervals to maximize power production efficiency. This places constraints upon unit construction costs, requiring lightweight structural cross sections that can ensure that fatigue strength meets the variable loads produced by constant power production, and in turn advanced design technology and precise analysis.

A chain mooring method was adopted for a FOWT stationkeeping system in the Fukushima FORWARD project, and NSE supervised research into mooring chain durability. NSE has previously been involved in mooring-

related design and construction, such as the development of floating fish-gathering buoys, multi-buoy moorings, and tethers for tension leg platforms (TLPs), as well as relevant research based upon the resulting technologies³⁾.

The use of chain mooring has a long record in construction projects. The specific method used in this development project is a spread mooring system with multiple mooring chains, providing a high degree of redundancy to achieve the required performance. The breakage of even one mooring chain due to a ship collision or other unexpected event should not result in any drifting. However, parts of the mooring chain may experience severe abrasion from marine environments. The degree of abrasion accounting for usage conditions has been specified in various design code references and standards, but no methods for calculating the abrasion amount have been established. Therefore, current design methods include regular inspection and maintenance, including replacement. The cost of such inspection and maintenance may impact total project costs. Therefore, there needs to be a comprehensive framework covering issues related to materials, design, construction, and maintenance. To this end, we have commenced research into identifying abrasion mechanisms through the evaluation of chain durability in order to improve life cycle costs, as well as research into creating methods to quantitatively calculate the abrasion amount and degree of fatigue damage. Furthermore, we have applied these calculation methods to measured data of floating substructure motions acquired during Fukushima FORWARD, calculated the abrasion amount and fatigue strength, and obtained findings useful to mooring design. The following sections summarize and report our findings.

2 Fukushima floating offshore wind turbine (FOWT) stationkeeping system




2.1 Overview of stationkeeping system

Table 1 shows the types and specifications of FOWT structures in Fukushima FORWARD. Three FOWTs with displacement of 5,000 to 30,000 tons were installed in a marine area with a water depth of approximately 120 m. The

mooring design was prepared by shipbuilding companies, and a spread mooring system using chain drag anchors was adopted. Fig. 1 shows a conceptual diagram of the spread mooring system. The floating substructures supporting the wind turbines were moored with multiple chains, which were each anchored to the seafloor by drag anchors. The chains were then connected to the FOWT via fairleads or equivalent to fairleads attached near the water surface to keep the FOWT in place. R3 or R3S stud-link mooring chains having a nominal diameter of 132 mm (the largest in Japan) were used.

There are critical design requirements for the proposed mooring system. It should maintain FOWT stationkeeping and ensure power generating performance for 20 years amid severe metocean conditions and an approximately 1,000 kN wind load from power production. Furthermore, the R3S offshore mooring chain and high-strength R5S chain have a long record as the standard mooring chains for oil and gas production facilities, and code references and standards set forth safety verification methods including analysis methods, safety factors, and inspection methods.

Table 1. Floating structures in Fukushima FORWARD

Name	Compact semi-sub.	V-shaped semi-sub.	Advanced spar
Power generation Capacity	2.0 MW	7.0 MW	5.0 MW
draft	19 m	17 m	33 m
Hub height	65 m	105 m	86 m
Mooring chain	6 lines, grade R3	8 lines, grade R3	6 lines, grade R3S
Schematic view			

From <http://www.fukushima-forward.jp/>

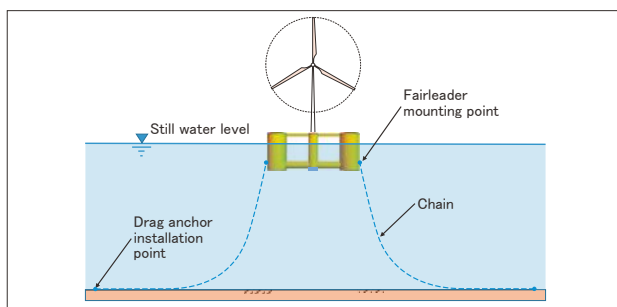


Fig. 1 Conceptual diagram of chain spread mooring system.

2.2 Mooring chain durability

2.2.1 Mooring chain durability, inspection, and maintenance

In a technology demonstration project in which the mooring chain was retrieved after use, there was significant abrasion of the chain link section several centimeters long at its touchdown point and at the fairlead connecting it to the floating substructure. However, other chain links reportedly showed almost no corrosive abrasion. The abrasion may be a consequence of the shaking of the floating substructure being absorbed by sliding of the joints. For example, in another case, there was significant abrasion of some chain links in a single-point mooring floating fish gathering buoy⁴⁾ installed in an area with a water depth of approximately 1000 m. It had been used for 10 years without maintenance because abrasion countermeasures were applied to specific sections at which abrasion occurs. According to recognized codes and standards related to mooring design⁵⁾, the corrosive abrasion allowance for chain links is considered at the time of design, and the structural integrity of mooring systems is ensured by repairing the chain link if abrasion is found to exceed the corrosive abrasion allowance during periodic inspections.

However, it is difficult to conduct inspections, maintenance, and repairs on FOWTs because of the limited space available for inspection and repair. Thus, there is a risk of considerably reduced fatigue strength owing to the progressive abrasion of some chain links. A comprehensive framework embracing issues related to materials, design, construction, and maintenance is therefore required.

2.2.2 Mooring chain behavior

To ascertain the durability of mooring chains, it is important to precisely estimate mooring chain behavior and tension during power production, and not only under storm conditions. FOWTs are simultaneously buffeted by forces and made to change direction from the wind, seas, swells, and currents. Furthermore, the behavior of stationkeeping mooring chains is extremely complicated owing to rapid changes in the wind load magnitude and direction triggered by sudden starts and stops in power production. During Fukushima FORWARD, the six

degrees-of-freedom (DoF) motions of each of the FOWTs were observed by GPS over a one-year period at sampling intervals of 0.02 to 0.05 s, including power production. This measured data on floating substructure motions is valuable globally, and can be used to ascertain the behavior of FOWTs and mooring chains at each instant.

3 Calculation of abrasion amount/fatigue strength

3.1 Development of calculation method

We developed a method for calculating the abrasion and fatigue strength of chain links. The steps are shown in Fig. 2.

(1) Use the six-DoF motion data on floating substructures measured by GPS to calculate the tension and inclination angle generated at each instant in the chain link.

(2) Calculate the slippage occurring in a chain link contact points, abrasion volume based on the Archard wear equation⁶⁾, and the abrasion depth generated in the chain link. Calculate the abrasion volume using the specific abrasion amount obtained from laboratory abrasion tests simulating marine environments using R3 or R3S-grade steel.

(3) Investigate the stress generation distribution state using the finite-element method (FEM) based on the abrasion depth, and thereby set the stress concentration factor.

(4) Use the stress concentration factor corresponding to the abrasion depth obtained based on (2) and (3) above to calculate the cumulative fatigue damage.

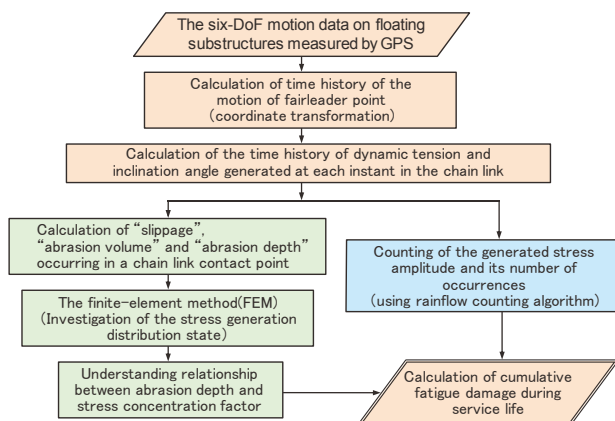


Fig. 2 Overall algorithm for fatigue damage calculation.

3.2 Calculation of abrasion amount

3.2.1 Abrasion amount equation

Here, we apply the Archard wear equation, which is an equation for calculating the abrasion amount in steel for general structures. We calculate the abrasion amount as the sum total of the abrasion amount based on the slippage ΔL generated in chain link contact points and the tension T generated between the links at each instant.

Eq. (1) yields the abrasion volume V_{Ab} that is generated when two pieces of steel are rubbed together with load T . This equation shows that V_{Ab} is proportional to the product of load T and slippage ΔL generated between the pieces; the constant of proportionality is therefore referred to as a specific abrasion amount Ws :

$$V_{Ab} = \sum (Ws \times T \times \Delta L) \quad (1)$$

3.2.2 Calculation of slippage between chain links

The calculation method for the slippage generated between links is shown below.

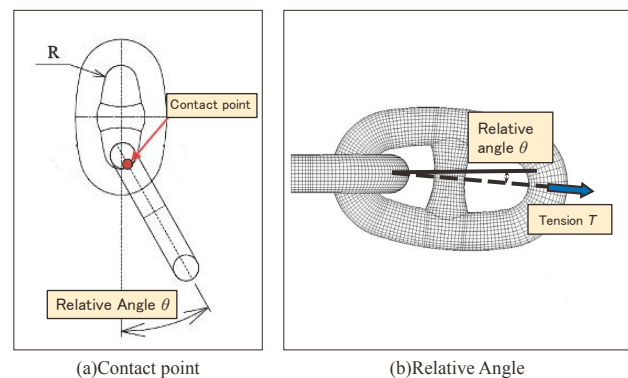


Fig. 3 Link contact point and relative angle between links.

(1) Slippage

The incremental slippage ΔL generated at a chain link contact point in incremental time Δt from time t can be calculated using Eq. (2) as the product of the absolute value of the incremental relative angle $\Delta\theta_r(t)$ between the chain links within the incremental time Δt and the inner radius R of chain links. Here, D_c is the nominal diameter of the chain link, and the inner radius R of the chain link is $0.65D_c$ specified by JIS standards.

$$\begin{aligned} \Delta L &= |\Delta\theta_r(t)| \times R \\ &= |\theta_r(t + \Delta t) - \theta_r(t)| \times 0.65D_c \end{aligned} \quad (2)$$

(2) Relative angle $\theta_r(t)$ between links

We assume the relative angle $\theta_r(t)$ to be the difference between the inclination angle $\theta_i(t)$ of the i^{th} chain link counting from the fairlead point at time t and the inclination angle $\theta_{i+1}(t)$ of the adjacent $(i+1)^{\text{th}}$ chain link, and we calculate it using Eq. (3).

$$\theta_r(t) = \theta_{i+1}(t) - \theta_i(t) \quad (3)$$

(3) Abrasion volume

Substituting Eqs. (2) and (3) into ΔL in Eq. (1), the abrasion volume V_{Ab} is obtained from the sum of the products of the specific wear amount W_s , tension T , and the incremental time of the relative angle $\theta_r(t)$, and it can be calculated using Eq. (4).

$$\begin{aligned} V_{Ab} &= \sum (W_s \times T \times \Delta L) \\ &= \sum (W_s \times T \times 0.65D_c \times |\Delta\theta_r(t)|) \\ &= \sum (W_s \times T \times 0.65D_c \times |\theta_r(t + \Delta t) - \theta_r(t)|) \\ &= \sum \{W_s \times T \times 0.65D_c \times |\theta_{i+1}(t + \Delta t) - \theta_{i+1}(t) - \\ &\quad (\theta_i(t + \Delta t) - \theta_i(t))|\} \end{aligned} \quad (4)$$

When a floating substructure is buffeted by waves and subject to rolling and swaying motions, the motion of each chain link alters the entire geometry of the mooring chains, and thus they smoothly move in tandem with the substructure to ensure effective stationkeeping. However, as shown by Eq. (4), when this occurs, there is a change of $\Delta\theta_r(t)$ in the relative angle between chain links as they receive tension T , and sliding corresponding to $0.65D_c \times |\Delta\theta_r(t)|$ occurs in the link contact points, resulting in the generation of accumulating abrasion.

(4) Calculation of relative angle $\theta_r(t)$ and tension $T(t)$ from catenary shape

The relative angle $\theta_r(t)$ and the generated tension $T(t)$ between chain links at a point and time (t) are necessary when calculating Eq. (4). Given the displacement coordinates $(X_o(t), Z_o(t))$ of a fairlead point, the relative angle $\theta_r(t)$ and the tension $T(t)$ generated in a chain link on a mooring chain at point $P(X_p(t), Z_p(t))$ can thus be calculated (as described in Section 5.1 below).

(5) Abrasion depth

Fig. 4 shows a model of the abrasion shape. If the volume of the shaded area in the figure is expressed by the function $V_m(d)$ with abrasion depth d as a variable, then the abrasion depth d can be obtained using an iterative calculation for convergence so that the abrasion volume V_{Ab} obtained in Eq. (4) equals the numerical expression $V_m(d)$.

Utsumi et al.⁷⁾ observed worn chain links in the offshore structure's retrieved mooring chains and referenced them when approximating the abrasion shape with a cosine function. This approximation is also adopted in the present study, and we express the abrasion range using $f(\theta)$ and θ_0 , which are defined by Eqs. (5) and (6), respectively, for the inner bend of the chain link.

$$f(\theta) = d \times \cos\left(\frac{\pi\theta}{2\theta_0}\right) \quad (5)$$

Using polar coordinates with point O on the center line of the chain link shown in Fig. 4 as a pole, we define the difference between the distance from point O to the worn part and the distance R to an intact chain link at angle θ as $f(\theta)$, and we define the range in which the angle $\theta \leq \theta_0$ as the abrasion range.

d : Abrasion depth at the inner end of the chain link

θ : Angle on the inside of the bend

θ_0 : Limit angle of abrasion defined by Eq. (6).

$$\theta_0 = \sin^{-1}\left(\frac{L}{R}\right) \quad (6)$$

L : Limit length generated by abrasion and assumed to be 66 mm (1/2 of the link diameter 132 mm) in this study.

R : Link inner radius ($0.65D_c$).

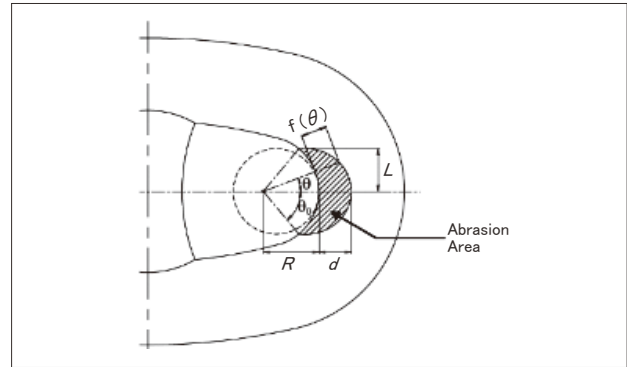


Fig. 4 Abrasion area

3.3 Specific abrasion amount according to laboratory tests

To determine the specific abrasion amount W_s defined in Eq. (1), Iwai et al.⁸⁾ conducted laboratory experiments on JIS S15C and S55C, carbon steel for mechanical structural use. However, the mechanical properties and alloy composition of the steel material are technically different from the grade R3S (KSBCR3S), which is the subject of the present study. Therefore, Nippon Steel Corporation conducted abrasion tests⁹⁾ in artificial seawater using a steel sample that was cut from a chain of the same material (grade R3S) as part of the Fukushima FORWARD.

3.3.1 Test method

Fig. 5 shows a schematic diagram of the test. The test piece (painted red in the figure) is slid at a constant amplitude and period under constant load T . Then, the abrasion amount is measured when a set number of slides is reached, and the relationship between the sliding distance and steel abrasion amount is evaluated.

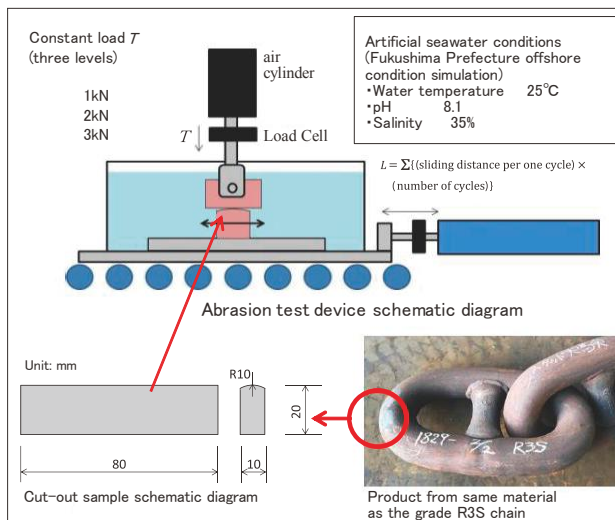


Fig. 5 laboratory abrasion test schematic⁹⁾.

3.3.2 Test results

Fig. 6 shows the effect of sliding distance on the specific wear amount using the results of the sliding experiment. The horizontal axis shows the sliding distance L (m), and the vertical axis shows the specific abrasion amount W_s defined in Eq. (1), with straight lines connecting the values obtained at each measurement point. The three curves with constant load T as a parameter shown in the figure

almost overlap and converge. Therefore, it can be inferred that the influence of the size of constant load T on the specific abrasion amount is small, and that the relational rule of Eq. (1), which states that the abrasion amount is proportional to the product of load T and sliding distance amount ΔL , is valid. It can be seen from the figure that the specific abrasion amount has a high value of $5 \times 10^{-6} \text{ mm}^3/(\text{N m})$ at the initial stage of abrasion, which gradually decreases, and approaches a constant value of $2 \times 10^{-6} \text{ mm}^3/(\text{N m})$. Furthermore, the specific abrasion amount of $2 \times 10^{-6} \text{ mm}^3/(\text{N m})$ at that time is very similar to the values in the literature⁸⁾ (JIS S15C and S55C, carbon steel for mechanical structural use). This implies that the steel type has minimal impact on the specific abrasion amount.

In addition, according to the measured data on floating substructure motions, the accumulated one-year sliding distance of each chain link with relatively large sliding motion, such as those reaching the seafloor, is approximately 600 m. The increase in abrasion in the first year is therefore relatively large. It may be estimated that the specific abrasion amount gradually approaches a constant value as the contact between steel materials settles into a steady state. This phenomenon can be explained by the fact that the abrasion amount is proportional to the surface pressure. The contact surface is divided into finite elements with very small cross-sectional area a ; therefore, the surface pressure on the finite element is uniform, and Eq. (1) holds even for the finite elements. When both sides of Eq. (1) are divided by the cross-sectional area a , the abrasion depth (left side of Eq. (1)) is shown to be proportional to the surface pressure T/a (right side of Eq. (1)). Irregularities in a contact surface promote the abrasion of finite elements with a large surface pressure, resulting

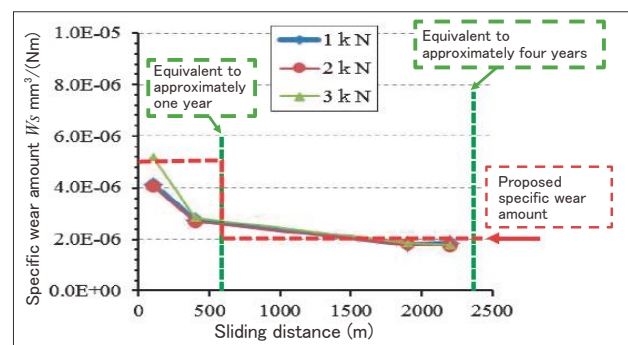


Fig. 6 Relationship between sliding distance and specific abrasion amount.

in a so-called smoothing effect in which an action occurs where the surface pressure on the entire contact surface is equalized.

3.4 Calculation of fatigue strength of links with significant abrasion

It is generally assumed that corrosion (uniform) and corrosive abrasion (local) occurs uniformly on the surfaces of chain links made of steel bars, and the cumulative fatigue damage is calculated using a fatigue strength curve ($T-N$ curve) having a cross section subtracting the corrosive abrasion allowance from the chain link diameter. For example, the corrosion and corrosive abrasion amount assumed during the period of use is set as the allowable corrosive abrasion, and the link is replaced if corrosion and the corrosive abrasion amount exceed the allowable corrosive abrasion. Generally, defects are considered insignificant relative to the cross section if the local corrosive abrasion is assumed to be small. Therefore, assuming that significant stress concentration does not occur, calculating the fatigue strength of a thinned cross section with uniform corrosive abrasion over the entire circumference of a steel bar is valid. However, for FOWTs, there may be constraints on mooring inspection and maintenance. Furthermore, if abrasion of contact points is large, significant stress concentration may occur owing to changes in the cross-sectional shape, and fatigue strength may decrease. Thus, a calculation method that also includes these conditions is needed.

3.4.1 Fatigue strength calculation method

When calculating the fatigue strength of mooring chains, we count the frequency of occurrence of tension fluctuation amplitudes, and then calculate the linear cumulative fatigue damage according to the Palmgren-Miner rule¹⁰). There are two methods of estimating the fatigue life of a mooring chain under variable load. The first is to calculate the amplitude of the generated tension ($T-N$ fatigue approach), and the second is to calculate the generated stress amplitude ($S-N$ fatigue approach). In each case, a fatigue strength curve showing the relationship between the number of repetitions of tension or stress and the allowable number of repetitions, is used. The number of repetitions of tension or stress amplitude counted under variable load is divided by the allowable number of repetitions to calculate the fatigue damage and fatigue life. Table 2 shows a typical fatigue strength curve used in different codes and standards. The $T-N$ fatigue approach was applied to the mooring design in Fukushima FORWARD. Although its practicalities, it cannot account for the stress concentration when chain abrasion has grown progressively larger, such as in fairleads or at chain touchdown points. Meanwhile, there are two different $S-N$ fatigue approaches: the first (hereinafter, $S-N$ fatigue approach (1)), uses a fatigue strength curve showing the relationship between the nominal stress amplitudes and the allowable number of repetitions $n_c(s)$. The second (hereinafter, $S-N$ fatigue approach (2)) calculates the fatigue damage using the stress concentration factor S_{cf} obtained by FEM analysis.

Table 2. Fatigue strength curves for different codes and standards.

Code and standard Name	Fatigue strength curve ($S-N$ curve and $T-N$ curve) The component capacity against tension fatigue
(1)DNV-OS-E301 POSITION MOORING	<u>$S-N$ fatigue approach ①</u> $n_c(s) \cdot s^m = a_b$ $n_c(s)$: the number of cycles (the allowable number of repetitions) s : the nominal stress range (double amplitude) <u>$S-N$ fatigue approach ②</u> Calculation using appropriate stress concentration factors (S_{cf}) obtained by a FEM and the B1 curve according to DNVGL-RP-C203
(2)API-RP-2SK Recommended Practice for Design and Analysis of Stationkeeping Systems for Floating Structures	<u>$T-N$ fatigue approach</u> $N \cdot R^m = K$ N : the number of permissible cycles of tension R : Ratio of tension range (double amplitude) to reference breaking strength (RBS).
(3)ISO 19901-7 Stationkeeping systems for floating offshore structures and mobile offshore units	<u>$T-N$ fatigue approach</u> $N \cdot T^m = K$ N : the number of permissible cycles of tension T : the ratio of tension range (double amplitude) to the reference breaking strength of the component <u>$S-N$ fatigue approach</u> $N \cdot S^m = K$ N : the number of permissible cycles of stress S : the stress range (double amplitude)

The S - N fatigue approach (2) is effective when using a new material or a shackle (DNV-OS-E301⁵⁾) for which a T - N curve has not been obtained. It can use a stress concentration factor S_{cf} and the fatigue strength curve of the material in response to the environment, or the shape of a material member.

In this study, we accordingly applied the S - N fatigue approach (2) and used FEM analysis to calculate stress distributions in a chain link that is assumed to be worn. We then calculated the fatigue damage in the chain by multiplying the local stress concentration factor S_{cf} obtained by the nominal stress amplitude S_N , using the B1 fatigue strength curve in the DNV-RP-C203 standard¹¹⁾ (for free corrosion, i.e., in seawater without corrosion protection).

$$S = S_N \times S_{cf} \quad (7)$$

Here, S : Local stress amplitude
 S_{cf} : Local stress concentration factor
 S_N : Nominal stress amplitude = $\Delta T / \text{Area}$
 ΔT : Tension amplitude
 Area : Cross-sectional area of chain link assuming uniform corrosion.

3.4.2 Stress concentration factor according to abrasion depth

FEM analysis was used to investigate the impact of the corrosive abrasion depth on the local stress concentration factor (S_{cf}), and to determine the relationship between the corrosive abrasion depth and stress concentration factor.

Fig. 7 shows an example of the circumferential direction distribution of maximum principal stress when a design load is acting upon the contact points between links with a uniform 2 mm corrosion and a 4 mm deep abrasion. The horizontal axis shows the position of the calculation point along the circumferential direction, and the vertical axis shows the maximum principal stress. The maximum principal stress is positive in the tensile state that affects crack growth; the blue-colored area in the figure indicates the range in which the links are in contact with each other, and the contact point is indicated

by a negative sign in the compressed state. The stress concentration factor was calculated by dividing the maximum value of the maximum principal stress of each part by the nominal stress (22.15 N/mm^2). The maximum stress concentration factor was generated in the bend part and had a value of 5.96.

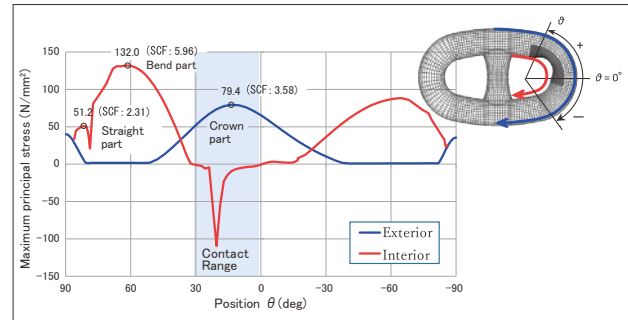


Fig. 7 Distribution of stress concentration factor along the circumferential direction.

Fig. 8 shows the change in the stress concentration factor at further abrasion depths of 0 mm, 6 mm, or 14 mm with uniform corrosion of 2 mm. The relationship between the maximum stress concentration factor and the amount of corrosive abrasion is shown for cases where the corrosive abrasion depth, which is the sum of the uniform corrosion of 2 mm and the abrasion depth, is 2 mm, 8 mm, and 16 mm, respectively. Here, a corrosive abrasion depth of 8 mm corresponds to the corrosive abrasion allowance for fatigue strength analysis when a structure is used for 20 years at a corrosive abrasion rate of 0.8 mm/year in the most severe corrosive abrasion environments, such as on the seafloor. (Annual corrosive abrasion rate of $0.8 \text{ mm/year} \times 20 \text{ years} \times 50\% = 8 \text{ mm}$).

The red dashed line in the figure is an approximate expression obtained from the relationship between the corrosive abrasion amount and the stress concentration factor for a corrosive abrasion amount of 16 mm or less. The stress concentration factor is found to be largely proportional to the corrosive abrasion amount. The blue solid line is a concave approximation curve bending downwards as the corrosive abrasion amount increases beyond 16 mm before reaching 24 mm. Meanwhile, the fatigue strength curve shown in Table 2 is typically $n(s) \cdot s^m = a_D$ (a_D , m : constants), and the allowable number of repetitions $n(s)$ is inversely proportional to the

power of the stress amplitudes. The fatigue strength is therefore inversely proportional to the power of the stress concentration factor. When the corrosive abrasion amount exceeds approximately 20 mm, the fatigue life decreases sharply. However, the relationship can be linear in the assumed range for the FOWT in Fukushima FORWARD (corrosive abrasion amount of 8 mm or less).

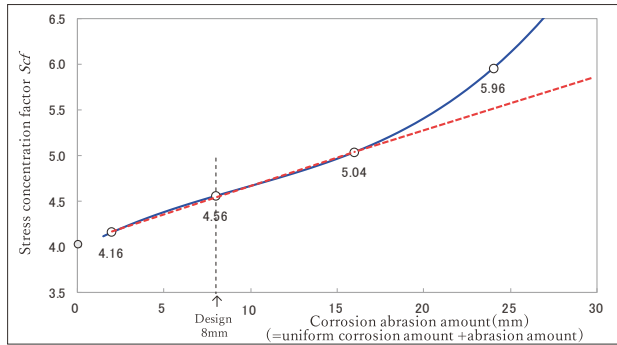


Fig. 8 Relationship between corrosive abrasion depth and stress concentration factor.

4 Abrasion and fatigue strength analysis based on measured data of floating substructure motions in Fukushima FORWARD

The corrosive abrasion amount and accumulated fatigue damage were calculated using the measured data of floating substructure motions in Fukushima FORWARD.

4.1 Investigation steps

GPS devices were used to continuously measure the motions of floating substructures in Fukushima FORWARD in the surge, sway, heave, roll, pitch, and yaw modes at 0.02 to 0.05 s intervals at the device mounting positions during a one-year period. The displacement at the fairlead mounting positions was calculated after converting the coordinates from the GPS mounting positions to fairlead mounting positions. The fairlead mounting positions and anchor positions were then used to calculate the tension generated in each mooring chain at each instant, as well as the inclination angle of each chain link and the slippage at contact points by catenary calculation. Abrasion depth corresponding to the

progression of abrasion was calculated using Eq. (1). The accumulated fatigue damage was also calculated using the stress concentration factor according to the cumulative abrasion in each link.

4.2 Calculation results

4.2.1 Calculation of abrasion amount and depth over one-year period

Fig. 9 shows the calculation results for the abrasion amount over a one-year period. The horizontal axis shows the length of mooring chains from fairlead positions, and the vertical axis shows the abrasion amount. The result shows the longitudinal distribution of the abrasion amount. Peaks are present near the fairleads and touchdown points. A peak value appears near the 230 m length position on the horizontal axis in the figure, and the section reaching approximately 50 m before and after this position corresponds to the touchdown point. The links repeatedly touchdown and float up from the seafloor, and the relative angle of links at their touchdown points changes discontinuously before and after touchdown on the seafloor. This increasingly accumulates the amount of slippage between links, resulting in a larger abrasion amount. The movement of the chain link is restricted at fairleads and touchdown points, so the slippage increases. The 20-year values of abrasion amount converted to abrasion depth are 7.1 mm for fairleads and 6.1 mm for touchdown points.

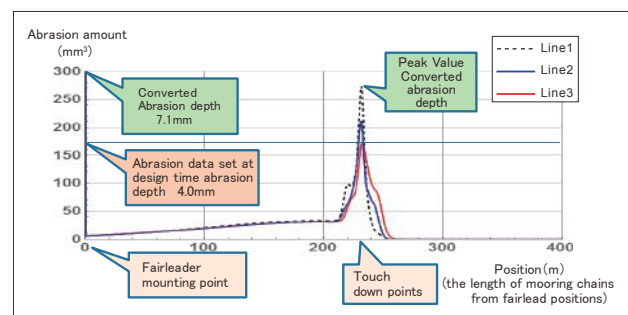


Fig. 9 Amount of abrasion distribution in longitudinal direction of mooring chain links.

Fig. 10 illustrates the extraction of the time points when the slippage increases the most throughout the year. The slippage increases during typhoons, which coincides with significant horizontal displacements of floating substructures. It is estimated that the horizontal

displacement of the floating substructure was absorbed by the sliding of each chain link of mooring chains, resulting in increased chain link abrasion.

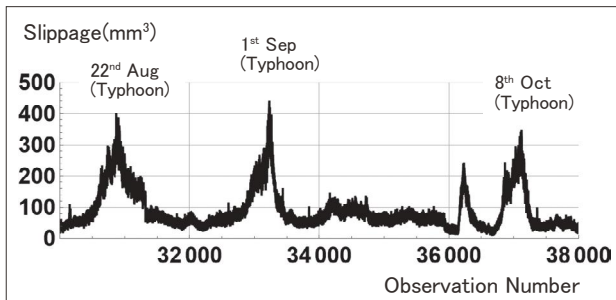


Fig. 10 Slippage calculations.

4.2.2 Cumulative fatigue damage

The generated stress amplitude and its number of occurrences were counted using the rainflow-counting algorithm⁽¹⁰⁾ for the time history of line tension. A histogram of the stress amplitude was created using the measured data of floating substructure motions.

Next, we calculated the cumulative fatigue damage using the *S-N* approach (2), multiplying the nominal stress by the stress concentration factor according to each abrasion depth. Particular consideration was given to the bending and out-of-plane sliding angle of the chain link at fairlead points. Thus, we selected links sliding according to the tension and release angle at each instant obtained using measured motion data, and then calculated the bending and out-of-plane sliding amount acting on those chain links. Furthermore, we calculated the abrasion amount and fatigue damage.

In Fig. 11, the horizontal axis shows the two variables of (1) chain link position and (2) generated stress amplitude level, and the corresponding cumulative fatigue damage is plotted on the vertical axis. The position of the chain link was indicated by the length based on the fairlead point. This is a bird's-eye view obtained from the results of measuring floating substructure motions at intervals of 0.02 s for approximately one year and has a naturally sculpted beauty. According to this figure, the "Length" at which fatigue damage reaches its maximum is approximately 130 m. However, because the "Length" to touchdown points is approximately 180 m, the maximum value position is near the seafloor and

slightly above touchdown points. The largest peak of cumulative fatigue damage appears in the 10 to 20 MPa stress amplitude range, which is generated by waves in the normal sea state; the second peak occurs near a stress amplitude of approximately 40 MPa, corresponding to typhoon conditions. We see here that large cumulative fatigue damage is the cumulative result of normal waves, which occur more frequently than the extreme waves arising from typhoons several times a year.

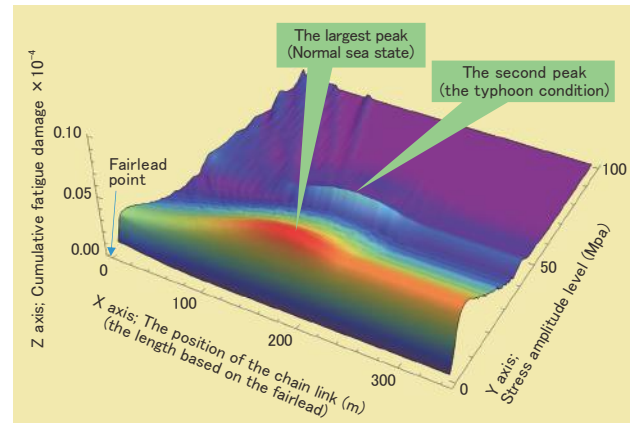


Fig. 11 Cumulative fatigue damage to chain link over a one-year period.

4.2.3 Effect of change in the floating substructure position owing to power production on cumulative fatigue damage

Fig. 12 shows a histogram of the occurrence frequency of planar floating substructure positions based on measured motion data and highlighting the presence or absence of power production (different from the FOWT in Fig. 11). The X and Y coordinate values of each point shown in Fig. 12 are the average values of the positions of the floating substructures every 10 min. Floating substructures experience more changes in their planar position during "(b) Power production" than "(a) No power production", and they also encounter greater movement.

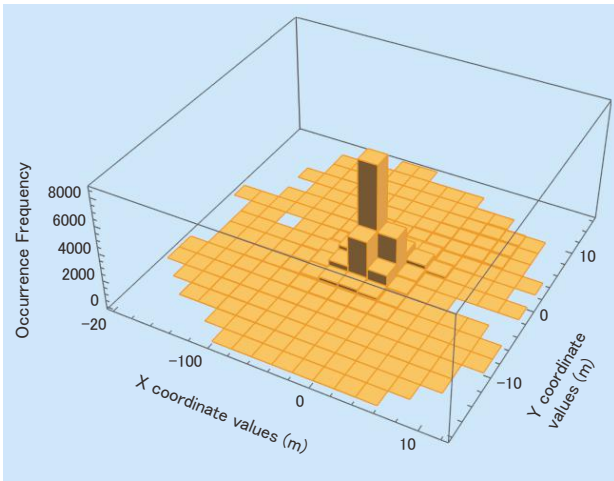
Figs. 13(a) and 13(b) show the lengths of mooring chains from fairlead points on the X-axis, the stress amplitude level on the Y-axis, and the cumulative fatigue damage on the Z-axis. Comparing Figs. 13(a) and (b), the effect of power production, parking, or idling on the degree of cumulative fatigue damage can be clearly seen. Fig. 13(a) covers all measured data, including during power production and parking, and the cumulative fatigue

damage due to stress with an amplitude level exceeding 100 MPa is high. Meanwhile, in Fig. 13(b), which only shows measured data when there is no power production (such as during idling), large stress amplitude levels do not predominate, and there is little overall cumulative fatigue damage.

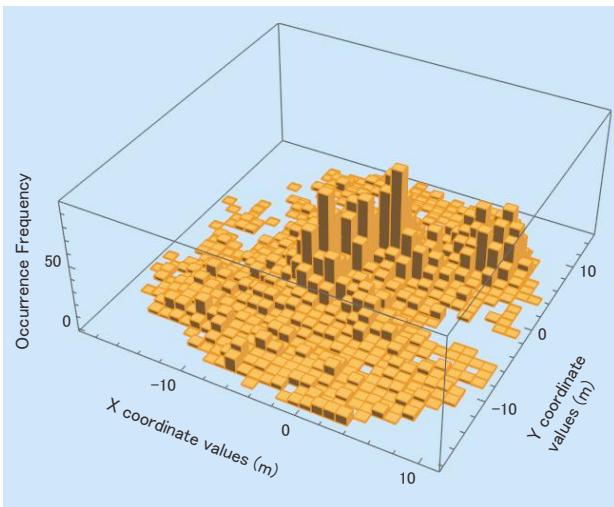
The distribution of the stress amplitude level changes owing to the movement of floating substructures in the horizontal plane. During power production, the positions of floating substructures due to wind load in the horizontal plane changes from upwind to downwind. Correspondingly, the fluctuation range of the mooring line tension becomes larger, and a stress amplitude level exceeding 100 MPa is produced. However, when there is no power production, a stress amplitude level of

approximately 50 MPa predominates.

There have been concerns that the abrasion amount would increase owing to the large change in the horizontal position of floating substructures caused by wind load during power production. However, it was found that the chain links subject to abrasion became dispersed as the touchdown points where abrasion should be concentrated fluctuate from moment to moment. Furthermore, calculations of the cumulative fatigue damage accounting for the local stress concentration occurring with the progressive abrasion of chain links showed a maximum value of 0.00576, so the FOWT in Fukushima FORWARD exhibited a sufficient fatigue strength over their 20-year service life.

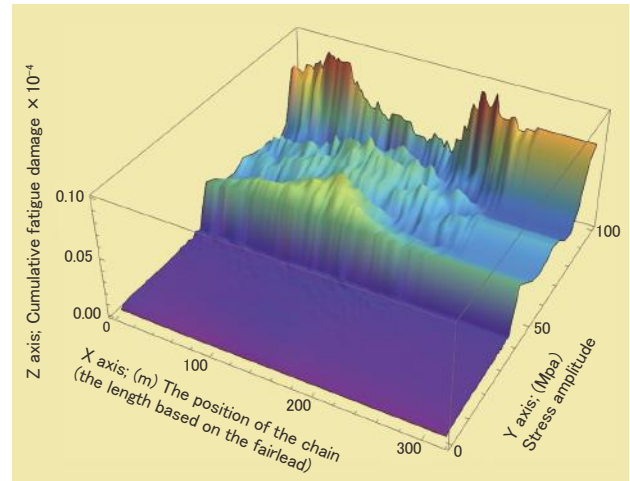


(a) No power production

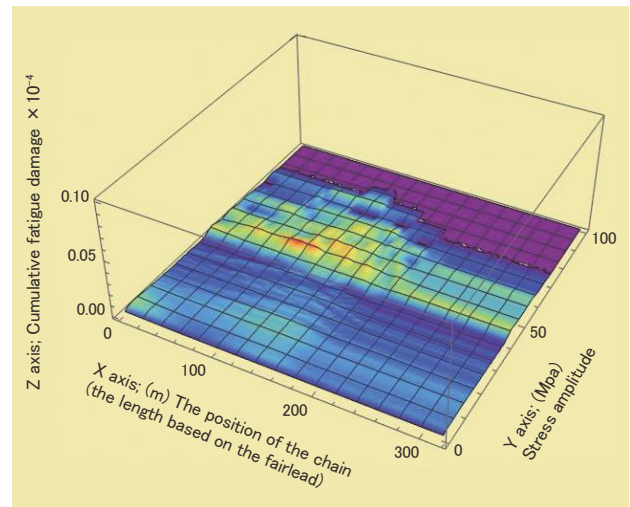


(b) Power production

Fig. 12 Histogram of floating substructure position in horizontal plane coordinates.



(a) All data targets, including during power production



(b) Targets only during non power production

Fig. 13 Annual Cumulative fatigue damage to chain link.

4.2.4 Effect of progressive abrasion on fatigue strength

We assumed the abrasion volume to be proportional to the number of years, based upon the results of abrasion volume estimated using the one-year continuous measurement data on the motions of floating substructures in Section 4.2.1. Calculating the abrasion depth for each year, we set the stress concentration factor according to the abrasion shape at those times, and then calculated the cumulative fatigue damage over the service life of the floating substructures. Eq. (8) shows the S - N curve used (corresponding to the B1 curve in the DNV-RP-C203 standard¹¹⁾).

$$\begin{aligned} \log_{10}(N_i) &= a_1 - m \times \log_{10}(\Delta s_i \times S_{cf}) \\ &= a_1 - m \times \log_{10}(\Delta s_i) - m \times \log_{10}(S_{cf}) \\ & \quad a_1, m; \text{constant} \end{aligned} \quad (8)$$

Figs. 14 and 15 respectively show changes in the abrasion depth and stress concentration factor over time, both of which increase in an almost flat convex curve.

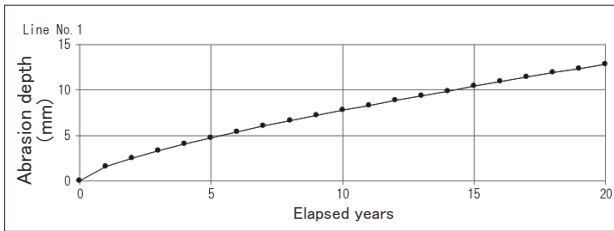


Fig. 14 Prediction of abrasion depth changes over time.

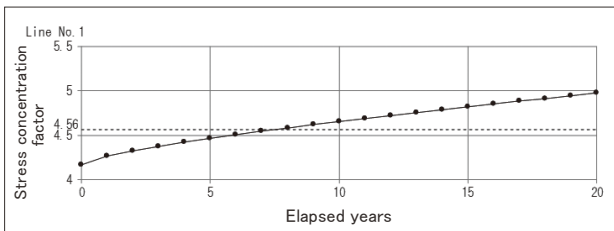


Fig. 15 Prediction of stress concentration factor changes over time.

4.2.5 Comparison of calculation methods in fatigue strength analysis

In the previous section, the yearly change of the abrasion depth of each chain link was set based on the amount of abrasion that was obtained from the measured data, and the stress concentration factor was obtained from FEM analysis. In this section, using these data the change in

the extent of cumulative fatigue damage of the chain link over time during the full service life is calculated.

(1) Calculation method:

There have been concerns about progressive abrasion causing shape defects that would lead to an increase in the stress concentration factor, thereby accelerating cumulative fatigue damage. It has been said that “fatigue analysis may consider 50% of chain corrosion allowance.”. This means that fatigue analysis uses thinned cross-sections, uniformly applying half of the total corrosive abrasion amount estimated during the period of use to the entire service life. In other words, fatigue damage is calculated by uniformly applying the abrasion amount for 10 years, which is the midpoint of a 20-year service life, or the average value during the period of use.

In the following section, we compare the cumulative fatigue damage results obtained from using the two methods. The second line of Eq. (8) shows that Δs_i and S_{cf} can be treated separately, resulting in Eq. (9).

$$\begin{aligned} N_i &= 10^{a_1 - m \times \log_{10} \Delta s_i} \times 10^{-m \times \log_{10} S_{cf}} \\ &= 10^{a_1 - m \times \log_{10} \Delta s_i} \times S_{cf}^{-m} \end{aligned} \quad (9)$$

The 20-year cumulative fatigue damage D_{20} can be calculated by Eq. (10) as the sum of the fatigue damage D_{jy} for each year. Here, $S_{cf,jy}$ in the equation is the stress concentration factor according to the cumulative abrasion depth over jy years.

$$\begin{aligned} D_{20} &= \sum_{jy=1}^{20} D_{jy} = \sum_{jy=1}^{20} \left(\sum_{i=1}^{N_i} \frac{n_i}{N_i} \right) \\ &= \sum_{jy=1}^{20} \left\{ \left(\sum_{i=1}^{N_i} \frac{n_i}{10^{a_1 - m \times \log_{10}(\Delta s_i)}} \right) \times S_{cf,jy}^{-m} \right\} \end{aligned} \quad (10)$$

The first term in the last line of Eq. (10) is the annual cumulative fatigue damage due to nominal stress, and the second term shows that the impact of local stress concentration caused by abrasion on fatigue damage is proportional to the power of the local stress concentration factor, and D_{20} can be calculated by multiplying each of these after separately calculating them as follows.

First, the frequency distribution of the nominal stress Δs of each link based on the line tension generated over a one-year period is calculated using the measured data of

each chain link of floating substructures, and the one-year fatigue damage D_1 on the intact chain link (i.e., when the chain link is not impacted by abrasion and the local stress concentration factor = 1.0) is calculated. Next, the annual amount of abrasion for each link is calculated, and the corresponding abrasion depth is used to calculate the local stress concentration factor $S_{cf,1}$. Finally, multiplying these two values gives the cumulative damage in the first year.

Furthermore, assuming that the marine environmental conditions will remain unchanged after the second year, the generated line tension frequency distribution, slippage between links, and abrasion volume generated each year are presumably the same throughout the 20-year service life, so the cumulative amount of abrasion is proportional to the number of years. The cumulative fatigue damage over time can be separately calculated in the form of a power of local stress concentration factor $S_{cf,jy}$ according to the abrasion depth in the jy^{th} year based on the second term in Eq. (10). This is then multiplied by the first year fatigue damage D_1 of an intact chain link.

Multi-year measured motion data on floating substructures is preferred although they are difficult to obtain in practice. The uncertainty lies in determining the validity of applying one-year marine environmental condition data to 20-year calculations. Normal waves contribute significantly to cumulative fatigue damage, as shown in Fig. 11, while the contribution from typhoons, despite their extreme stress amplitudes, is relatively small. However, changes in the wave energy state of marine areas are small compared to changes over time caused by typhoon-scale events or path changes. This means that the impact of changes from marine phenomena over a 20-year period on cumulative fatigue damage is minimal. Therefore, it is reasonable to assume that actual conditions will not deviate from the above assumption that the marine environmental conditions experience during the one-year period of floating substructure measurements will subsequently continue.

[Method-1] Use the representative local stress concentration factor (refer to DNV standards)

$$D_{20} = 20 \times S_{cf}^m \times D_1 \quad (11)$$

Here, the local stress concentration factor $S_{cf} = 4.56$ is uniformly used throughout the service life period (used for 20 years on the entire chain length).

This value ($S_{cf} = 4.56$) is the local stress concentration factor obtained by FEM analysis with a uniform corrosion depth of 2 mm and an abrasion depth of 6 mm at the midpoint of service life.

[Method-2] Use the local stress concentration factor for each year according to abrasion depth

$$D_{20} = \sum_{k=1}^{20} D_k = D_1 \times (S_{cf,1}^m + S_{cf,2}^m + \dots + S_{cf,20}^m) \quad (12)$$

Here,

D_1 : One-year cumulative fatigue damage (stress concentration factor 1.0, assuming intact chain links without corrosive abrasion) according to chain link measured data

D_k : Cumulative fatigue damage in the k^{th} year ($k \geq 2$)

$S_{cf,k}$: Local stress concentration factor in the k^{th} year.

(2) Calculation results:

Fig. 16 shows an example of the longitudinal distribution of the cumulative fatigue damage to a mooring chain. The figure shows the results calculated using [Method-1] (applying Eq. (11) with a representative local stress concentration factor), which are somewhat safer than using [Method-2] (applying Eq. (12)), and have somewhat larger fatigue damage. Assuming representative dimension d for abrasion depth, the corresponding abrasion volume is roughly proportional to the cube of d , so the abrasion depth d is roughly proportional to the cube root of the abrasion volume. This is because if the abrasion volume increases constantly, abrasion depth d increases slowly compared to [Method-1], which uniformly uses the 10th year abrasion estimate (the midpoint of service life) and assumes a constant increase and larger cumulative fatigue damage. In addition, the section of the red line in the figure encircled by the blue frame indicates the point at which the cumulative fatigue damage is slightly increasing. This corresponds to a touchdown point close to a 175-m length on the horizontal axis, and indicates a high frequency of chain link touchdown, as well as

increased cumulative fatigue damage due to progressive chain link abrasion at the touchdown point. In terms of the entire length of the mooring chain, there is little increase, and the effect of progressive abrasion on fatigue strength is small in general areas other than the touchdown point. Furthermore, the maximum fatigue damage is slightly closer to the fairlead point than the touchdown point, whereas the maximum abrasion amount is near the touchdown point. The positions of the sites where maximum values occur differ in each case, which is a desirable result in terms of fatigue strength.

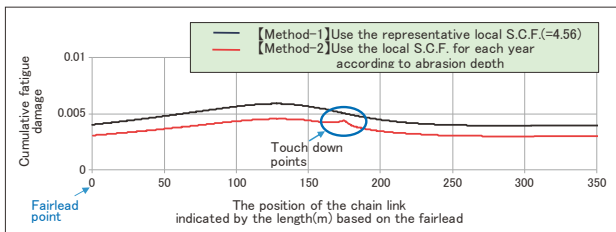


Fig. 16 Longitudinal distribution of cumulative fatigue damage on mooring chain links.

5 Dynamic mooring line tension in stationkeeping design

It is important to handle the dynamic behavior (line dynamics) of the mooring chain itself, and the analysis method and its applicability are described. The impact of line dynamics on stationkeeping design in Fukushima FORWARD is not large, so quasi-static analysis was used.

5.1 Quasi-static analysis, dynamic analysis, and approximate calculation method

5.1.1 Handling of line dynamic analysis methods in rules of recognized classification societies

In the design and analysis of stationkeeping systems for floating substructures, we performed response analysis that considered the interaction between floating substructures and stationkeeping systems comprising mooring chains and anchors. The specifications of the chains were designed such that the safety factor (i.e., the allowable tension/maximum tension predicted by mooring line response analysis) is less than the required

safety factor according to the design criteria of recognized classification societies.

Table 3 classifies mooring line response analysis methods, and it also presents the target loads and the order of mooring line motion modes for each analysis method. The required safety factor⁵⁾ is set according to the tension estimation accuracy of each mooring line response analysis method in each code and standard.

Table 3. Classification of mooring line response analysis methods.

Name of analysis methods	Target loads acting on line	The order of mooring line motion modes
(1)Quasi-static analysis	buoyancy,gravity	first-order
(2)Approximate calculation method	buoyancy,dead weight, inertial force,dynamic fluid force	first-order
(3)Dynamic line response analysis	same as above	higher-order

5.1.2 Quasi-static analysis

Fig. 17 is a model diagram showing a state in which the upper end of a mooring chain is assumed to be hanging from a fairlead point, and the other end is to be anchored to the seafloor in a slack condition, keeping the mooring line tangential to the seafloor at the touchdown point. The figure shows the mechanical equilibrium of the mooring line components (length ds) corresponding to each chain link of the mooring chain at that instant. In a stationary state, the catenary (suspension line) is formed in a state where the dead weight, buoyancy acting on the mooring chain components, and tension T acting on both ends of each component are statically balanced. When the fairlead point slowly moves in the horizontal direction away from the anchor (red dashed line in the figure), the line tension gradually increases owing to the sequential rise in the line component weight from the seafloor. Furthermore,

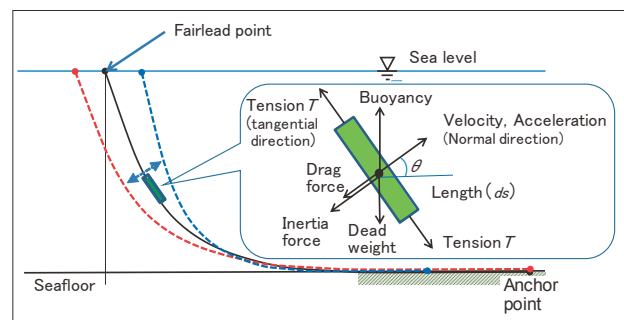


Fig. 17 Model diagram showing the equilibrium of the mooring line components.

the inclination angle $\theta(t)$ of the mooring chain becomes smaller; for this reason, the horizontal component $\cos\theta(t)$ of the line tension increases, thereby becoming the restoring force against the horizontal movement of the fairlead point. In this way, the pseudo-static balance is maintained at each instant, and the fluctuating line tension generated at that time is defined as the quasi-static restoring force. An analysis method that assumes a pseudo-static balance is called quasi-static analysis.

5.1.3 Basic catenary equation

The basic catenary equation is described below.

Fig. 18 shows the statically balanced state of each chain link. When the chain link length is ds , the underwater weight per unit length ('weight in air' – buoyancy) is w , the inclination angle is θ , the line tension acting on the upper and lower chain link ends is $T + dT$ and T , respectively, and the horizontal component of the line tension is T_H ; then, the equilibrium equation in the vertical direction is given by Eq. (13). The horizontal component T_H of the tension ($=T\cos\theta = (T + dT)\cos(\theta + d\theta)$) becomes a constant value regardless of the position of the mooring chain, and T_H is used in Eq. (13) given the ease of subsequently expanding the equation.

$$T_H \times \tan(\theta + d\theta) - T_H \times \tan(\theta) = w \times ds \quad (13)$$

When $T_H \times \tan(\theta + d\theta)$ is expanded into a Taylor series and linearly approximated, then

$$\begin{aligned} T_H \times \frac{d(\tan\theta)}{d\theta} d\theta &= w \times ds \\ T_H \times \frac{1}{\cos^2\theta} d\theta &= w \times ds \end{aligned} \quad (14)$$

Here,

$$ds = \sqrt{dx^2 + dz^2} = dx \sqrt{1 + \left(\frac{dz}{dx}\right)^2} \quad (15)$$

If Eq. (15) is substituted into Eq. (14), then

$$T_H \times \frac{1}{\cos^2\theta} d\theta = w \times dx \sqrt{1 + \left(\frac{dz}{dx}\right)^2} \quad (16)$$

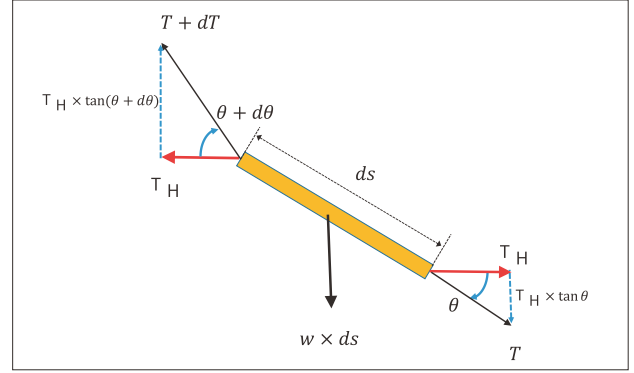


Fig. 18 Static equilibrium diagram of mooring chain links.

Here,

$$\frac{d^2z}{dx^2} = \frac{d}{dx} \left(\frac{dz}{dx} \right) = \frac{d(\tan\theta)}{d\theta} \frac{d\theta}{dx} = \frac{1}{\cos^2\theta} \frac{d\theta}{dx} \quad (17)$$

In addition, when Eq. (16) is substituted into Eq. (17) and re-arranged, then the ordinary differential equation shown in Eq. (18) is obtained. Here, a is defined as the value of the horizontal component T_H of the tension at the fairlead point ($T\cos\theta$) divided by the unit weight w of the chain underwater ($a = T_H/w$), and is a constant value at a position on the mooring chain.

$$\begin{aligned} \frac{d^2z}{dx^2} &= \frac{1}{\cos^2\theta} \frac{d\theta}{dx} = \frac{w}{T_H} \times \sqrt{1 + \left(\frac{dz}{dx}\right)^2} \\ &= \frac{1}{a} \sqrt{1 + \left(\frac{dz}{dx}\right)^2} \end{aligned} \quad (18)$$

Here, Fig. 19 shows the definition of the coordinates. When the boundary conditions of Eq. (19) are the distance from the anchor point to the touchdown point (landing length) b and touchdown point z -coordinate value 0, and the mooring chain is tangential to the seafloor at the touchdown point, gradient 0 is substituted into Eq. (18), obtaining catenary equation shown in Eq. (20).

$$z(b) = 0; \quad \left. \frac{dz}{dx} \right|_{z=0} = 0 \quad (19)$$

Furthermore, substituting the obtained Eq. (20) into Eq. (15) results in Eq. (21). Eqs. (20) and (21) are the basic catenary equations.

When the position coordinates of a point on a mooring chain forming a catenary shape (suspension line) are (x, z) , the length of the mooring chain from the anchor point

is l , and the landing length on the seafloor is b ; then, z and l can be expressed by a function with x , a , and b as variables by Eqs. (20) and (21).

$$z = a \left\{ \cosh \left(\frac{x-b}{a} \right) - 1 \right\} \quad (20)$$

$$l = a \sinh \left(\frac{x-b}{a} \right) + b \quad (21)$$

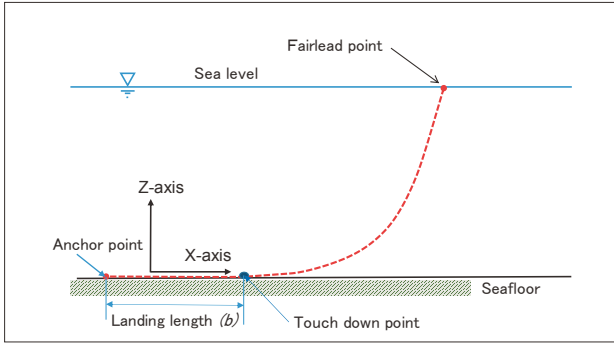


Fig. 19 Coordinate definition diagram.

When the lengths from anchor points to the fairlead points are $l = l_0$, $x = x_0$, and $z = z_0$, and a minute displacement is assumed in Eqs. (20) and (21), then Eqs. (22) and (23) can be derived, and C_{rest} in Eq. (22) becomes a static restoring force matrix at fairlead points, which is shown in Eq. (23). C_{rest} is used in the approximate calculation method, which is a one-line dynamic response analysis that is described later. Furthermore, when conducting an integrated response analysis of a wind turbine, tower, floating substructure, and stationkeeping system under the effects of wind and wave loads, then C_{rest} corresponds to the stiffness elements constituting the overall stiffness matrix of a stationkeeping system used when calculating the natural resonance period of horizontal motion (surge, sway, yaw). Furthermore, a large amount of time is needed for the time-domain analysis of the wind turbine, floating substructure, and stationkeeping system, so frequency-domain analysis is effective, and C_{rest} can be used for the required linearized stationkeeping characteristics.

$$\begin{bmatrix} da \\ db \end{bmatrix} = C_{rest} \begin{bmatrix} dx_0 \\ dz_0 \end{bmatrix} \quad (22)$$

$$C_{rest} = \frac{1}{D} \begin{bmatrix} \sinh B_0 & \cosh B_0 - 1 \\ -\cosh B_0 & \sinh B_0 - B_0 \cosh B_0 \end{bmatrix} \quad (23)$$

$$D = 2 + B_0 \sinh B_0 - 2 \cosh B_0; \quad B_0 = \frac{x_0 - b}{a}$$

5.1.4 Dynamic line response analysis

In Fig. 17, when a fairlead point oscillates at a high frequency, the velocity and acceleration generated in each element of the mooring chain become large, and the inertial force and fluid force acting on each element are more prominent than the dead weight of the mooring chain. The line tension fluctuation caused by this inertial force or fluid force is called “dynamic fluctuation tension”, the analysis methodology is “dynamic response analysis” and the dynamic effect of the mooring chain is “line dynamics”.

Fig. 20 shows the time history of the line tension generated when a sinusoidal forced oscillation, which simulates the movement of a fairlead point caused by the motions of a floating substructure, is applied to the fairlead point. In the figure, the time history of the line tension fluctuation according to dynamic response analysis obtained using OrcaFlex¹²⁾ is shown with a solid line, and the time history obtained by quasi-static analysis is also shown by a dashed line. OrcaFlex can handle the dynamic response of flexible structures underwater based on the structural FEM method, and has been used in the fatigue strength investigation of riser power cables in Fukushima FORWARD. When focusing on the peak points of the line tension wave shape obtained by the dynamic response analysis in the figure and comparing it to the quasi-static analysis results, it can be seen that its value is large, its waveform is split, and its phase is delayed by approximately 90° . It can be estimated that the influence of line dynamics causes high-frequency oscillations owing to the secondary oscillation mode of the mooring chain and the non-linearity of the drag term¹³⁾.

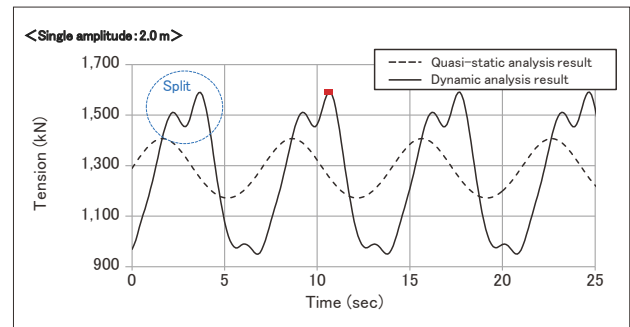


Fig. 20 Time-history response diagram showing calculated results of mooring line dynamic tension.

5.1.5 Approximate calculation method

Ando et al.¹⁴⁾ proposed a simple and practical method to analytically calculate the inertial force and fluid force acting on mooring chains. This method is based on the catenary theory, and is referred to as the approximate calculation method in source text. An overview of this calculation method is shown below. Fig. 21 shows the definitions of the coordinates and symbols of the catenary shape.

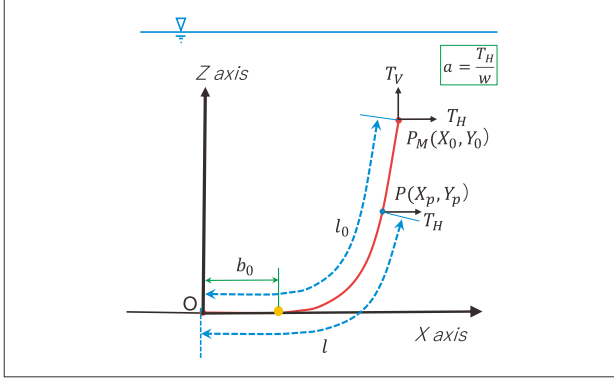


Fig. 21 Definition diagram of catenary coordinates and symbols.

When the coordinates of a fairlead point P_M are set as (X_0, Z_0) , and the point P_M is forced to move slowly to coordinates $(X_0 + \Delta X_0, Z_0 + \Delta Z_0)$, then the mooring chain is assumed to be maintaining the shape of a catenary, and so any point $P(X_p, Z_p)$ that moves on the mooring chain is also above the newly formed catenary. This implies the imposition of the kinematic condition that each element of a mooring chain is on the catenary when moving.

The point $P(X_p, Z_p)$ is on the catenary, and the horizontal component T_H of the tension has the same value as the fairlead point P_M , so Eqs. (20) and (21) hold, and Eqs. (24) and (25) can be derived by solving simultaneous equations Eqs. (20) and (21).

$$X_p = a \times \sinh^{-1} \left(\frac{l-b}{a} \right) + b \quad (24)$$

$$Z_p = a \left(\sqrt{\left(\frac{l-b}{a} \right)^2 + 1} - 1 \right) \quad (25)$$

Here, it is assumed that the horizontal component T_H of the tension on the fairlead point P_M changes by a minute amount ($\Delta T_H = \Delta a \times w$), and the landing length on the seafloor changes by Δb . At this time, X_p and Z_p are

regarded as functions of the variables a and b in Eqs. (24) and (25). The variable l showing the element position is set as a constant and a first-order approximation in the Taylor expansion is applied, which allows for Eqs. (26) and (27) to be derived. A matrix display is performed as shown in Eq. (28), and the degree of change ($\Delta X_p, \Delta Z_p$) of the mooring line element P point (X_p, Z_p) can be expressed by the linear transformation of Δa and Δb , which is defined by the fairlead P_M point.

$$\Delta X_p = \frac{\partial X_p}{\partial a} \Delta a + \frac{\partial X_p}{\partial b} \Delta b = 0 \quad (26)$$

$$\Delta Z_p = \frac{\partial Z_p}{\partial a} \Delta a + \frac{\partial Z_p}{\partial b} \Delta b = 0 \quad (27)$$

$$\begin{pmatrix} \Delta X_p \\ \Delta Z_p \end{pmatrix} = \begin{pmatrix} \frac{\partial X_p}{\partial a} & \frac{\partial X_p}{\partial b} \\ \frac{\partial Z_p}{\partial a} & \frac{\partial Z_p}{\partial b} \end{pmatrix} \begin{pmatrix} \Delta a \\ \Delta b \end{pmatrix} \quad (28)$$

When the transformation matrix of Eq. (28) is set as matrix $S(l)$, whose variable is the length l indicating the position of each element of a mooring chain, then when each component is arranged by partially differentiating Eqs. (24) and (25), Eq. (29) can be obtained and Eq. (28) is expressed as Eq. (30).

$S(l)$

$$= \begin{pmatrix} \sinh^{-1} A(l) - \frac{A(l)}{\sqrt{1+A(l)^2}} & \frac{A(l)}{\sqrt{1+A(l)^2}} - 1 \\ \frac{1}{\sqrt{1+A(l)^2}} - 1 & \frac{1}{\sqrt{1+A(l)^2}} \end{pmatrix} \quad (29)$$

$$\text{where } A(l) = \frac{(l-b)}{a}$$

$$\begin{pmatrix} \Delta X_p \\ \Delta Z_p \end{pmatrix} = S(l) \begin{pmatrix} \Delta a \\ \Delta b \end{pmatrix} \quad (30)$$

Here, a mooring chain is divided and discretized into elements (length ds) equivalent to a chain link. For elements that are in the i^{th} position from the anchor point, the length from the anchor point is set as l_i , and the displacement amount from the equilibrium point is set as $(\Delta X_i, \Delta Z_i)$. At this time, the incremental displacement amount $(\Delta X_0, \Delta Z_0)$ at a fairlead point can be converted to $(\Delta a, \Delta b)$ by using Eq. (22); furthermore, Eq. (31) can be obtained by using Eq. (30), to linearly transform $(\Delta X_0, \Delta Z_0)$ to $(\Delta X_i, \Delta Z_i)$. The quasi-static restoring force matrix

C_{rest} . (Eq. (23)) and matrix $S(l)$ (Eq. (29)) with respect to length l expressing the position of a mooring chain is multiplied by the displacement $(\Delta X_0, \Delta Z_0)$ from the equilibrium point of a fairlead point. Variable l_i of matrix $S(l_i)$ is a number that identifies an element's position and is thus independent of time, and matrix C_{rest} is a constant regardless of an element's position l_i , and it is independent of time. Therefore, on the right side of Eq. (31), only $(\Delta X_0, \Delta Z_0)$ is time-dependent. The time-differentiation of both sides of Eq. (31) enables the calculation of velocity (V_{xi}, V_{zi}) using Eq. (32), and by time-differentiating both sides of Eq. (32), the acceleration (A_{xi}, A_{zi}) of the line i^{th} position elements can be expressed by Eq. (33).

$$\begin{pmatrix} \Delta X_i \\ \Delta Z_i \end{pmatrix} = S(l_i) \times Crest. \times \begin{pmatrix} \Delta X_0 \\ \Delta Z_0 \end{pmatrix} \quad (31)$$

$$\begin{pmatrix} V_{xi} \\ V_{zi} \end{pmatrix} = S(l_i) \times Crest. \times \frac{d}{dt} \begin{pmatrix} \Delta X_0 \\ \Delta Z_0 \end{pmatrix} \quad (32)$$

$$\begin{pmatrix} A_{xi} \\ A_{zi} \end{pmatrix} = S(l_i) \times Crest. \times \frac{d^2}{dt^2} \begin{pmatrix} \Delta X_0 \\ \Delta Z_0 \end{pmatrix} \quad (33)$$

The inclination angle θ_i of an element at the i^{th} position on a mooring chain is used to convert the above-mentioned values to velocity (V_{Ti}, V_{Ni}) and acceleration (A_{Ti}, A_{Ni}) in the tangential and normal directions of the element coordinate system. The basic Eqs. (20) and (21) show that the inclination angle θ_i of each element i of a mooring chain is $\tan(\theta_i) = dz/dx = \sinh((x-b)/a) = (l_i-b)/a$, and therefore $\tan(\theta_i) = (l_i-b)/a$ can be expressed as being equal to a function $A(l_i)$ of the length l_i showing the position of element i using $A(l) = (l-b)/a$, as defined in Eq. (29). Furthermore, Eq. (34) is used to calculate the viscous drag force dF_{dNi} , acting on each element, and is proportional to the square of velocity V_{Ni} in the normal direction of each element of a mooring chain, and inertial force dF_{mNi} due to inertia and added mass proportional to acceleration A_{Ni} in the normal direction. The fluid forces acting on each element are then added over the entire length of the mooring chain to numerically calculate the mooring force acting on a fairlead point. The accuracy can be ensured without performing convergence calculations for each time step, which is conducted by the implicit method of dynamic analysis. In Eq. (34), C_d

is the drag coefficient, D_e is the equivalent diameter of a cylinder equal to the displaced volume of a chain link accounting for the chain shape, w_a is the chain weight per unit length in air, C_a is the added mass coefficient of an equivalent cylinder, r_w is the weight of seawater, and G is gravitational acceleration.

As described above, the derivation and expansion of the basic equation of the approximate calculation method are slightly complicated, but this method can significantly reduce the required time to calculate by using the analytical solution together with the assumption of linear approximation.

$$dF_{dNi} = drag \times V_{Ni} |V_{Ni}| \times ds$$

$$drag : 1/2 \times \rho \times C_d \times D_e \quad D_e : \text{equivalent diameter} \quad (34)$$

$$dF_{mNi} = -Iner \times A_{Ni} \times ds$$

$$Iner : \left(w_a + C_a \times r_w \frac{\pi D_e^2}{4} \right) / G$$

5.1.6 Applicability of approximate calculation method

The features and applicability of this approximate calculation method are shown below.

The influence of dynamic fluctuating tension depends on the water depth and floating substructure motion characteristics. Marine areas where water depth exceeds 1,000 m involve long mooring lines with increased weight. The inertial force and fluid force generated in a mooring line itself becomes relatively large owing to the quasi-static restoring force, and the higher-order motion modes become dominant, making dynamic analysis necessary. Meanwhile, relatively shallow waters of approximately 100 m involve low-frequency motion for floating substructures, and mooring chains change shape slowly, resulting in a relatively small dynamic fluctuating tension. At the same time, the designs of stationkeeping systems for FOWTs require the use of a structural dynamic model and a time-history response analysis integrating the floating substructure, tower, wind turbine, and stationkeeping system. The inclusion of fatigue analysis and application of dynamic analysis to mooring chain results in a considerable computational time.

Fukushima FORWARD involves a relatively shallow

design water depth of approximately 120 m and a long period of motion in the horizontal plane for FOWTs, so the dynamic fluctuating tension is assumed to be small. Therefore, quasi-static analysis was used in the design of stationkeeping systems. Furthermore, investigations of chain durability, which is the subject of the present study, were conducted using the approximate calculation method instead of dynamic analysis.

As described above, it is reasonable to use different analysis methods depending on the water depth and motion characteristics of FOWTs; therefore, the line dynamics discrimination indicators are described below.

5.2 Line dynamics discrimination indicators

A discrimination indicator categorizing the impact of line dynamics in a simple manner was proposed as follows. Each component of the drag force resulting from viscous fluid force, inertial force, and static restoring force causing the generation of dynamic fluctuating tension was calculated in a simple manner, and their change tendencies were investigated based on the approximate calculation method.

5.2.1 Existing discrimination indicators

The influence of line dynamics differs greatly between deep and shallow water. Suhara et al.¹⁵⁾ focused on the acceleration of fairlead points to determine the influence of line dynamics and presented a discrimination indicator that covered deep water. The variable α was made dimensionless by dividing the acceleration A_{cc} at fairlead point by the gravitational acceleration G . The former is expressed as product of the fluctuation amplitude ΔZ_0 and the square of the angular frequency ω of the movement at the fairlead point. The equation is as shown in Eq. (35). Multiplying the mooring line mass by α results in the inertial force generated in the entire mooring line.

$$\alpha = \frac{A_{cc}}{G} = \frac{\Delta Z_0 \times \omega^2}{G} \quad (35)$$

Here, $\alpha = 1$ corresponds to acceleration $A_{cc} = G$, i.e., the free-fall state of the chain link.

Furthermore, Suhara et al.¹⁵⁾ also studied the snap

phenomenon seen in deep water. Here, when some chain links cannot follow the movement of a fairlead point, then the minimum tension becomes zero, i.e., the chain link is in a free-fall condition. If the movement of a fairlead is reversed when the chain link is in a free-fall state, a snap load occurs and propagates over the entire mooring line. This sequence of events occurs in each cycle, and the delimiter of the range where this so-called snap condition occurs was set by the above authors as discrimination indicator α_s . This indicator shows a tendency for the maximum tension to increase considerably beyond α_s , and is a useful indicator that captures the essence of the characteristics of line tension.

Fig. 22 shows the dimensionless acceleration α at a fairlead point on the horizontal axis and the maximum and minimum tension on the vertical axis based on the dynamic analysis results obtained by OrcaFlex, referring to a paper by Suhara et al.¹⁵⁾. In addition, it shows the impact of the acceleration generated at a fairlead point on line tension. The generated tension tends to increase with α generated in the fairlead point. Furthermore, the quasi-static analysis results are shown by the dashed lines in the figure, and the range where the quasi-static analysis results exceed the dynamic analysis results (i.e., the range where quasi-static analysis is valid) is shown in blue. Furthermore, the α value for which the dynamic analysis result and quasi-static analysis result are equal is shown as α_e in the figure.

In Suhara et al.¹⁵⁾, the inertial force of the line and the quasi-static restoring force were compared for the indicator showing that the application range of quasi-static analysis is valid. When α was used as a variable, the inequalities Eqs. (36) or (37) were set as the applicable ranges of quasi-static analysis, and the threshold value α , which has an equal sign in Eq. (37), was defined as α_H in Eq. (38).

$$\begin{aligned} & \text{line mass } (M) \times \text{dimensionless acceleration } (\alpha) \\ & \leq \text{quasi-static restoring force } (QSRF) \quad (36) \end{aligned}$$

Here, the line mass (M) is the sum of the mass of a mooring line and added mass (component of fluid pressure acting on line elements proportional to acceleration and

opposite in sign), and can be expressed as the product of $Iner$ shown in Eq. (34) and mooring line length S_0 .

$$S_0 \times Iner \times \alpha \leq \text{quasi-static restoring force (QSRF)} \quad (37)$$

$$\alpha_H = \frac{\text{quasi-static restoring force (QSRF)}}{\text{line mass}(M)} = \frac{QSRF}{S_0 \times Iner} \quad (38)$$

$$S_0 = \int ds : \text{mooring line length} \quad (39)$$

In Fig. 22, α_H is also indicated.

When $\alpha < \alpha_H$, the quasi-static restoring force is dominant, the tension fluctuation is stable, and the tension estimation accuracy is high. The installation water depth at the Fukushima FORWARD site is approximately 120 m, and it can be inferred from the motion resonance period of the floating substructures that this is within the applicable conditions of quasi-static analysis.

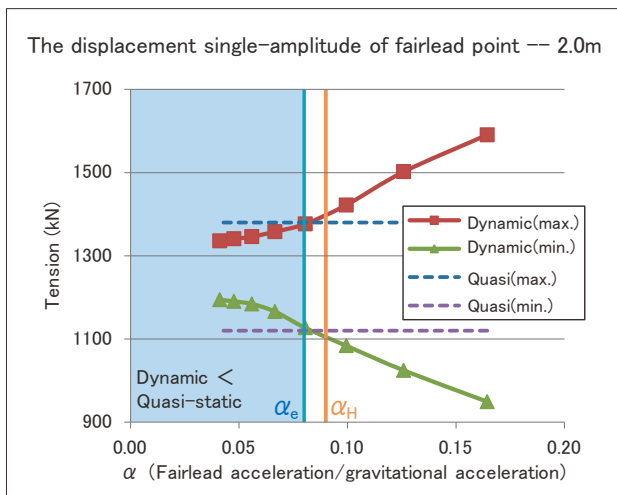


Fig. 22 Periodic dependence of dynamic fluctuating tension.

5.2.2 Proposal of revised indicator (revised α_H)

In the section above on existing discrimination indicators, the acceleration was included, but the velocity dependence of fairlead points was not. Meanwhile, the length of one mooring chain in Fukushima FORWARD was approximately 700 m, and the drag force, which is proportional to the square of the velocity of the mooring chain element, is important owing to the viscous fluid force acting on the mooring chain itself. Furthermore, in dynamic analysis results obtained using OrcaFlex, the tension fluctuation depends on the degree of displacement

amplitude amount of a fairlead point. Fig. 23 shows an example where the displacement single amplitude of the fairlead point was 6 m, focusing on the range of $\alpha < \alpha_H$, which differs significantly from that of Fig. 22, where the displacement single amplitude was 2 m. A value of 6 m for the displacement single amplitude is large, and may be such an extreme assumption that it is not applicable to the amount of fairlead movement of the FOWT in Fukushima FORWARD. Fig. 23 shows that dynamic analysis results greatly exceeded the quasi-static analysis results in the range of $\alpha < \alpha_H$, where existing indicators show quasi-static analysis to be applicable. Furthermore, the value of α defined in Eq. (35) has a linear relationship with respect to the displacement amplitude ΔZ_0 , so the displacement amplitude dependence cannot be sufficiently explained.

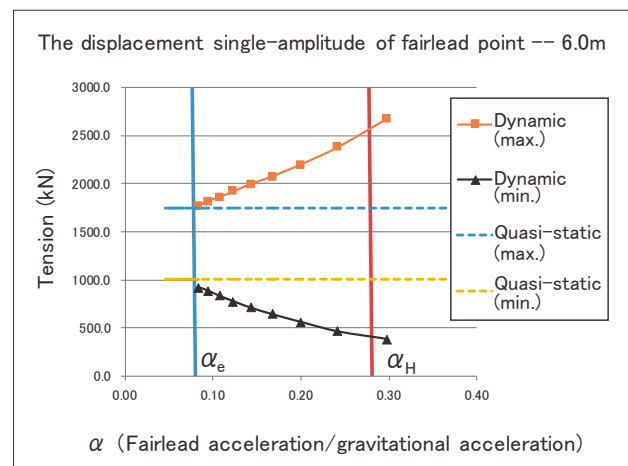


Fig. 23 Amplitude dependence of dynamic fluctuation tension.

Explaining the displacement amplitude dependence requires the incorporation of a second-order non-linear drag force term. Therefore, we investigated a revised indicator that incorporated the drag force term.

Fig. 24 shows the changes in the three components of dynamic tension [static restoring force term (1), drag force term (2), and inertial force term (3)] calculated by varying the frequency oscillation at a fairlead point. The analysis results by OrcaFlex (hereinafter, “dynamic tension”) are plotted with black circles together with the total absolute value of each component, referred to as the total value = $|\text{term (1)}| + |\text{term (2)}| + |\text{term (3)}|$. The symbol $|\#|$ indicates the absolute value of $\#$. The composite value refers to the largest of the values between

the static restoring force term (1) + inertial term (3) and drag force term (2), which consider the phase difference of each component as shown below. Considering each component in phase space, when the displacement of a reference fairlead is on a real axis in the phase plane, the restoring force term (1) and inertial force term (3) are out-of-phase, and they are on the same real axis in the phase plane and simultaneously produce a maximum and can be grouped together. Meanwhile, the drag force term (2) is almost in-phase with velocity ($i\omega\Delta X_0$), and has a phase delay of 90° with respect to the displacement (this is the main reason why in Fig. 20, the phase of dynamic tension lags with that of the displacement ΔX_0 by approximately 90°), and is on an imaginary axis in phase space. The two grouped values are therefore almost orthogonal in phase space. From this, drag force term (2) was isolated, restoring force term (1) + inertial force term (3) and drag force term (2) were compared, the larger value was taken as shown in formula $\text{Max}[\text{term}(1)+\text{term}(3),\text{term}(2)]$, and this was set as the composite value. The total value, which is the sum of the absolute values of the three components, is an excessive value because it does not consider the fact that there are phase differences between each component. The composite value captures the tendencies of the dynamic tension, which is the calculation result obtained by OrcaFlex. The dynamic tension value is between the composite value and the total value, and the upper and lower limit values can be ascertained. Here, the restoring force term (1) is the quasi-static analysis result. Given the above, the method for determining the applicability of quasi-static analysis and dynamic analysis is shown below.

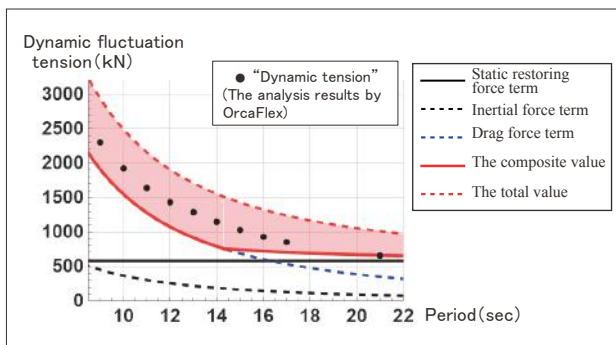


Fig. 24 Frequency dependence of each component of dynamic tension.

The inequality shown in Eq. (40) is used as the determination equation based on the lower limit value that is the composite value. This inequality compares the quasi-static restoring force and the composite value. The composite value is the lower limit value of the dynamic fluctuation tension, so the dynamic fluctuation tension \geq composite value \geq quasi-static restoring force. If the inequality in Eq. (40), i.e., composite value \geq quasi-static restoring force, is established, then the inequality: dynamic fluctuation tension \geq quasi-static restoring force is also established automatically, and a safe determination is thus given. Eq. (40) can be described as shown in Eq. (41) using α . The symbol $\text{Max}[* , \#]$ in Eq. (41) indicates that the larger of the two values in the square brackets $[\]$ is selected. The inequality in Eq. (41) involves the drag term (equal to $\alpha \times \text{drag} \times \Delta X_0 \times G = \Delta X_0 \times \omega^2 / G \times \text{drag} \times \Delta X_0 \times G = \omega^2 (\Delta X_0)^2 \times \text{drag} = V_0^2 \times \text{drag}$) being added to the left side of Eq. (37). This is the source of discrimination indicators in the existing paper. In Eq. (41), if only α is extracted to the left side, then Eq. (42) can be obtained. The α value that results in an equality in Eq. (42) is set as the [revised α_H]. The area framed by the blue line in Eq. (42) is the parameter α_H shown in Eq. (38). Here, ΔX_0 is the displacement at a fairleads point. The degree of the response displacement of the fairlead point is obtained by performing time-domain simulations under wind and wave conditions, where the wind turbine, tower, floating substructure, and stationkeeping system are integrated using the overall mooring stiffness (relationship between floating substructure displacement and mooring restoring force) obtained by quasi-static analysis. For reference, we use two indicators calculated¹³⁾ and compared in Fig. 23 above: α_e (for which quasi-static analysis and dynamic analysis results coincide at 0.05) and α_H (which becomes very large at 0.27), while the [revised α_H] is 0.07, and is shown to be more effective. Calculating the indicator [revised α_H] in Eq. (43) results in a guide for determining, in a relatively simple manner, the degree of influence of line dynamics¹³⁾.

$$\begin{aligned} & [\text{Composite value}] (\text{larger value of line inertia force or drag force}) \\ & \geq \text{quasi-static restoring force (QSRF)} \quad (40) \end{aligned}$$

$$\begin{aligned} S_0 \times \alpha \times \text{Max}[\text{Iner}, \text{drag} \times \Delta X_0 \times G] \\ \geq \text{quasi-static restoring force (QSRF)} \quad (41) \end{aligned}$$

$$\alpha \geq \frac{\text{QSRF}}{S_0 \times \text{Iner}} \times \frac{1}{\text{Max}\left[1, \frac{\text{drag} \times G \times \Delta X_0}{\text{Iner}}\right]} \quad (42)$$

$$[\text{revised } \alpha_H] = \alpha_H \times \frac{1}{\text{Max}\left[1, \frac{\text{drag} \times G \times \Delta X_0}{\text{Iner}}\right]} \quad (43)$$

5.2.3 Line dynamics of the FOWT in Fukushima FORWARD.

We target the incorporation of 2 to 7 MW wind turbines in the Fukushima FORWARD project having a displacement of 5,000 to 30,000 tons. The expected natural resonance period of rigid body motion was 10 s or more. Furthermore, floating substructure motions are inhibited owing to power production constraints, so it is inferred that motions at fairlead points are small and within the applicable range of quasi-static analysis.

6 Conclusion

Wind farms comprise a large number of FOWTs, each of which consists of floating substructures, wind turbines, and stationkeeping systems. The reliability of each stationkeeping system, mooring chain line, or single chain link forming a mooring chain line significantly affects the overall reliability and economic efficiency. In the present study, we developed a mooring chain durability evaluation method and provided a scientific basis for empirical aspects of abrasion.

The present study sought to analyze the risks introduced by each process of materials, design, manufacturing, construction, inspection, and maintenance to the overall project. In addition, the possibility of simultaneously improving the trade-off between economic efficiency, including lifecycle costs and structural reliability, by extensively investing in chain abrasion countermeasures at the design stage was investigated.

To the best of our knowledge, the evaluation of durability using data from continuous measurements of the six DoF motions of floating substructures conducted in this study is the first of its kind worldwide. The aim was to use durability evaluation and digital transformation technologies to realize advancements in design. The proposal of the Fukushima FORWARD project is to use data on floating substructure motions measured during service life to determine chain link abrasion, cumulative fatigue damage, and soundness during periods of use. This will be used to predict risks and can serve as a risk-based method that integrates design, inspection, and maintenance. In future, we hope that the results of this study will be verified by experiments (including demonstrations), incorporated into various codes and standards, lead to improved reliability and economic efficiency by minimizing lifecycle costs, and contribute to the realization of commercial wind farms.

Acknowledgments

This study was conducted as part of the “Demonstration Study on Steel Materials for FOWTs and Study on Life Evaluation of Mooring Chains” in the Fukushima FORWARD project¹⁾. We would like to express our gratitude to the Fukushima Offshore Wind Consortium, which provided the research opportunity, as well as to Professor Takeshi Ishihara, Department of Civil Engineering, School of Engineering, The University of Tokyo; Professor Hideyuki Suzuki, Ocean Space Planning Laboratory, Department of Systems Innovation, Graduate School of Engineering, The University of Tokyo; and Former Project Researcher Kiyokazu Yago, Graduate School of Frontier Sciences, The University of Tokyo, who were members of the Fukushima Offshore Wind Consortium and who provided detailed information and guidance; Mitsui Engineering & Shipbuilding Co., Ltd., Mitsubishi Shipbuilding Co., Ltd., and Japan Marine United Corporation, which provided the measured data of floating substructure motions and stationkeeping system design insight; and other associated individuals. We would also like to express our gratitude to the employees of the Nippon Steel Corporation for providing data on the laboratory sliding test and consideration of abrasion.

References

- 1) Fukushima Offshore Wind Consortium; Fukushima Floating Offshore Wind Farm Demonstration Project. <http://www.fukushima-forward.jp/index.html>
- 2) Ookubo H.; "Design and construction of floating foundations," *Wind Energy*, 37(4), Volume 108, February 2013.
- 3) Torii M., Yamazaki S., Sasaki N., Ookubo H., Yamashita A., Sakai K., Iwamoto C.; "Development of advanced mooring system for offshore floating wind turbine," *Nippon Steel & Sumikin Engineering Co., Ltd. Technical Review Vol. 6* (2015).
- 4) Surface steel floating fish reef, *Nippon Steel Engineering Technical Report Vol. 13* (2021).
- 5) DET NORSKE VERITAS; Position Mooring DNV-OS-E301
- 6) Archard equation. <https://en.wikipedia.org/wiki/Archardequation>.
- 7) Utsumi H., Sekita K., Nitta H.; "Stress concentration analysis of anchor chains subjected to abrasion or corrosion," *Proceedings of Civil Engineering in the Ocean*, 15:249-254, 1999.
- 8) Iwai Y., Itoh K., Gotoh K.; "Wear behavior of carbon steels and stainless steels in NaCl or Na₂SO₄ solution," *Transactions of the Japan Society of Mechanical Engineers Series C*, 62(601):248-255, 1996.
- 9) "Demonstration project of floating offshore wind power generation system off the shore of Fukushima" research report; "(3) Commercialization risk extraction / analysis and reduction method investigation: steel materials" *Nippon Steel & Sumitomo Metal*; Published May 2019; p.70-72 report_2017.pdf (meti.go.jp).
- 10) Japan Society of Materials Science (ed.), *Handbook of Fatigue Design*, 3rd Edition, published by Yokendo.
- 11) DET NORSKE VERITAS AS; DNV-RP-C203; "Fatigue Design of Offshore Steel Structures."
- 12) OrcaFlex Orcina HP: <https://www.orcina.com/SoftwareProducts/OrcaFlex/>
- 13) Michihiro A., Ootake A., Ookubo H., Suzuki H., Tokuda E.; "Dynamic behavior of mooring lines on floating wind turbine," *Journal of Japan Society of Civil Engineers, Ser. B3 (Ocean Engineering)*, 73(2):719-724, 2017.
- 14) Andoh S.; "Static tension characteristics and dynamic fluctuation characteristics of iron chain mooring line;" Kato S., ed., *Transactions of the West-Japan Society of Naval Architects*, 66:191-207, 1983.
- 15) Suhara T., Koterayama W., Tasai F., Hiyama H., Sao K., Watanabe K.; "Dynamic behavior and tension of oscillating mooring chain," *OTC4053*, 1981.